

# Nanoscale

Accepted Manuscript



This is an *Accepted Manuscript*, which has been through the Royal Society of Chemistry peer review process and has been accepted for publication.

*Accepted Manuscripts* are published online shortly after acceptance, before technical editing, formatting and proof reading. Using this free service, authors can make their results available to the community, in citable form, before we publish the edited article. We will replace this *Accepted Manuscript* with the edited and formatted *Advance Article* as soon as it is available.

You can find more information about *Accepted Manuscripts* in the [Information for Authors](#).

Please note that technical editing may introduce minor changes to the text and/or graphics, which may alter content. The journal's standard [Terms & Conditions](#) and the [Ethical guidelines](#) still apply. In no event shall the Royal Society of Chemistry be held responsible for any errors or omissions in this *Accepted Manuscript* or any consequences arising from the use of any information it contains.

Cite this: DOI: 10.1039/c0xx00000x

www.rsc.org/xxxxxx

ARTICLE TYPE

# Gold and gold-palladium alloy nanoparticles on heterostructured TiO<sub>2</sub> nanobelts as plasmonic photocatalysts for benzyl alcohol oxidation†

Tongtong Jiang<sup>a</sup>, Chuancheng Jia<sup>b</sup>, Lanchun Zhang<sup>a</sup>, Shuren He<sup>a</sup>, Yuanhua Sang<sup>c</sup>, Haidong Li<sup>c</sup>, Yanqing Li<sup>c</sup>, Xiaohong Xu<sup>\*a</sup> and Hong Liu<sup>\*c</sup>

Received (in XXX, XXX) Xth XXXXXXXXX 20XX, Accepted Xth XXXXXXXXX 20XX  
DOI: 10.1039/b000000x

Plasmonic photocatalysts composed of Au and bimetallic Au-Pd alloy nanoparticles (NPs) on one-dimensional TiO<sub>2</sub> nanobelt (TiO<sub>2</sub>-NB) were used for aerobic oxidation of benzyl alcohol under visible light irradiation. Remarkable light-promoted activity was observed for the as-synthesized M/TiO<sub>2</sub>-NB (M = Au, Au-Pd) nanostructures based on TiO<sub>2</sub>(B)/anatase heterostructured nanobelt. The difference in band structure and the well matched interface between TiO<sub>2</sub>(B) and anatase phases, coupled with the one-dimensional nanostructure, enable an enhanced charge transfer within the heterostructured nanobelt. This inter-phase charge transfer greatly facilitates the flow of hot electrons from metal NPs to TiO<sub>2</sub> and promotes benzyl alcohol oxidation. This efficient electron transfer was identified by the much higher photocurrent response measured for Au/TiO<sub>2</sub>-NB nanostructure with TiO<sub>2</sub>(B)/anatase heterojunction than those with either of the single phases under visible light irradiation. The alloying Au with Pd in Au-Pd/TiO<sub>2</sub>-NB results in a significant improvement in the visible light-promoted activity as compared to monometallic Au/TiO<sub>2</sub>-NB sample. It is supposed that the plasmon-mediated charge distribution within alloy NPs is mainly responsible for the enhanced photocatalytic activity of bimetallic nanostructures.

## 1. Introduction

It is always a challenge to develop environmentally benign catalytic process with high product selectivity. In the past decades, the rapid expansion of gold (Au) catalysis has developed many new approaches to achieve the chemical transformation under milder reaction conditions, such as low temperature CO oxidation,<sup>1-3</sup> propene epoxidation,<sup>4-6</sup> aerobic oxidation of alcohols and other organic matters.<sup>7-10</sup> However, some of these reactions are energy intensive and the product selectivity is relatively low. Fortunately, the conduction electrons of Au resonating with visible light (localized surface plasmon resonance, LSPR) can generate hot electrons and holes which can drive chemical reactions at room temperature with high product selectivity.<sup>11</sup>

Plasmonic-metal/semiconductor heterojunction structures, such as the integration of Au NPs with titanium dioxide (TiO<sub>2</sub>), have been proved to be promising visible light-driven photocatalysts.<sup>12-</sup>

<sup>17</sup> It has been shown that the ideal Au/TiO<sub>2</sub> plasmonic photocatalysts must allow an efficient separation and transfer of the photoinduced charge carriers, which is advantageous to achieve the high efficiency of plasmon-mediated catalysis

process.<sup>18</sup> When irradiated with visible light, the hot electrons excited in Au NPs can be injected into the conduction band of TiO<sub>2</sub> over the Schottky barrier, thus the separation of photoinduced charge carriers can be achieved.<sup>19-21</sup> However, the hot electrons transfer would lead to an electron accumulation in the conduction band of TiO<sub>2</sub>, which would prohibit the consecutive electron transfer from Au NPs to TiO<sub>2</sub>.<sup>18,22</sup> It is essential to promote the charge transfer within TiO<sub>2</sub> to smooth the injection of hot electrons. As reported in the literature, the mixed TiO<sub>2</sub> phases, such as the well-known P25 composed of anatase and rutile phases, exhibited superior photocatalytic activity to either of the component phases.<sup>23</sup> It is believed that the promoted charge transfer between different TiO<sub>2</sub> phases resulted from the difference between their band structure accounts for the excellent photocatalytic performance.<sup>24-26</sup> In fact, the structure of TiO<sub>2</sub> indeed has also shown a strong impact on the photocatalytic activity of plasmonic Au/TiO<sub>2</sub> catalysts by mediating the transfer of hot electrons.<sup>18,27,28</sup> For example, Hirai et al found that Au NPs located at the interface of anatase and rutile in P25 are much more efficient for aerobic oxidation of benzyl alcohol than those on pure anatase and rutile TiO<sub>2</sub> owing to the consecutive electron

transfer in this heterojunction.<sup>27</sup> One-dimensional TiO<sub>2</sub> nanobelts which are synthesized by the controllable hydrothermal method can readily form a heterostructure composed of anatase and the metastable phase TiO<sub>2</sub>(B) by controlling the calcination temperature of H<sub>2</sub>Ti<sub>3</sub>O<sub>7</sub> nanobelts.<sup>29</sup> Just like the case of P25, TiO<sub>2</sub>(B)/anatase heterostructure with coherent boundary bicrystalline has shown enhanced photocatalytic activity due to the efficient inter-phase charge transfer.<sup>29-34</sup> Moreover, compared with nanoparticles, the special one-dimensional nanostructure of TiO<sub>2</sub> nanobelts and nanorods would lead to a distinctive electronic properties, like free transport of electrons with a high speed along with the axial direction.<sup>35-37</sup> As a result, the efficient electron transfer within TiO<sub>2</sub> nanobelts can be expected. Furthermore, the TiO<sub>2</sub> nanobelts obtained by hydrothermal method normally have clean and smooth surfaces, which can highly disperse the catalytically active metal NPs or clusters.<sup>38,39</sup>

As is well known, for conventional heterogeneous catalysis, the bimetallic catalysts often show tunable and synergistic effect compared to their monometallic counterparts.<sup>40-42</sup> Moreover, it has been shown that the incorporation of a second metal can also effectively improve the photocatalytic performance of Au-based plasmonic photocatalysts.<sup>43-48</sup> Some of bimetallic nanostructures, such as Au-Pt,<sup>43</sup> Au-Cu,<sup>44</sup> Au-Ag<sup>45,46</sup> and Au-Pd<sup>47,48</sup> NPs supported on TiO<sub>2</sub>, exhibited much higher light-promoted activity for various chemical reactions than their monometallic counterparts.

Herein, Au and Au-Pd alloy NPs which are highly dispersed on TiO<sub>2</sub> nanobelts were synthesized. As expected, the visible light-promoted activity of Au/TiO<sub>2</sub>-NB photocatalysts strongly depends on the structure of TiO<sub>2</sub> nanobelt, and the highest activity enhancement for benzyl alcohol oxidation was obtained with TiO<sub>2</sub>(B)/anatase heterostructured nanobelt under visible light irradiation. Compared to monometallic Au/TiO<sub>2</sub>-NB sample, the alloying Au with Pd in bimetallic Au-Pd/TiO<sub>2</sub>-NB nanostructures resulted in improved catalytic activity. The photoelectrochemical measurement was used to discern the role of plasmon-mediated electron transfer process in the light-promoted activity of M/TiO<sub>2</sub>-NB photocatalysts.

## 2. Experimental section

### 2.1 Materials

H<sub>2</sub>Ti<sub>3</sub>O<sub>7</sub> nanobelts were synthesized via a typical hydrothermal process in concentrated NaOH aqueous solution with commercial P25 (Evonik, 50m<sup>2</sup> g<sup>-1</sup>, 80% Anatase, 20% Rutile) as the starting

material.<sup>29</sup> Calcining the H<sub>2</sub>Ti<sub>3</sub>O<sub>7</sub> nanobelts at 673, 873 and 1173 K, TiO<sub>2</sub> nanobelts with different structure were obtained, which were labeled as T-1, T-2 and T-3, respectively. HAuCl<sub>4</sub> and PdCl<sub>2</sub> (Acros Chemicals) were used as gold and palladium precursors. Urea of analytical reagent grade was used as the precipitation agent. All of the reagents were directly used without further treatment. Ultrapure water was used throughout our experiments.

### 2.2 Synthesis of M/TiO<sub>2</sub>-NB nanostructures

**Au/TiO<sub>2</sub>-NB:** These nanostructures were synthesized by the deposition-precipitation method. 0.1 g TiO<sub>2</sub> nanobelts were dispersed evenly in 50 ml aqueous solution comprising HAuCl<sub>4</sub>. Subsequently, a designated amount of urea with a metal/urea molar ratio at 1/200 in 100 ml water was added as the precipitation agent. Thereafter, the suspension was thermostatically held at 353 K and kept constant for 6 h under vigorous magnetic stirring in the absence of light. After the deposition-precipitation procedure, the resulting product was filtrated and washed with ultrapure water for several times. The filter cake was dried at 353 K under air for 12 h and then was calcined at 673 K for 2 h with a 5 K min<sup>-1</sup> heating rate under N<sub>2</sub> flow.

**Au-Pd/TiO<sub>2</sub>-NB:** A range of bimetallic Au-Pd/TiO<sub>2</sub>-NB nanostructures were synthesized by the similar method of Au/TiO<sub>2</sub>-NB nanostructures, but PdCl<sub>2</sub> with a controlled Au/Pd molar ratio was added and the dry filter cake was calcined at 673 K under H<sub>2</sub> flow.

In all nanostructures, subscript numbers denote the molar fractions of Au or Pd which are calculated on the basis of the metal atom amount in precursor suspension.

### 2.3 Characterization

The metal loading was detected with an inductively coupled plasma spectrometer (ICP-AES) on an IRIS Intrepid II XSP instrument (Thermo Electron Corporation). X-ray diffraction (XRD) analysis was conducted on a German Bruke D8 Advance powder X-ray diffractometer with Cu-K $\alpha$  ( $\lambda = 0.15406$  nm). Transmission electron microscopy (TEM) and high resolution transmission electron microscope (HR-TEM) images were obtained with a JOEL JEM 2100 microscope. The UV-visible (UV-vis) absorption spectra were recorded on a Shimadzu U-2400PC spectrophotometer with barium sulfate as the standard for the background correction. X-ray photoelectron spectroscopy (XPS) data were acquired on a Thermo ESCALAB 250 X-ray photoelectron spectrometer and the binding energies were

determined utilizing C1s spectrum as reference at 284.6 eV.

## 2.4 Catalytic reaction test

The photocatalytic activities of the as-synthesized M/TiO<sub>2</sub>-NB nanostructures were estimated via the aerobic oxidation of benzyl alcohol under visible light irradiation. The catalyst (20 mg) was dispersed well by ultrasonication in 5 ml toluene containing 40 μmol benzyl alcohol within a Pyrex glass tube (15 mm in diameter with a capacity of 20 ml). After purging the suspension with O<sub>2</sub> for 5 min, the tube was sealed with a rubber septum cap. The irradiation was carried out under vigorous magnetic stirring for 5 h using a 500 W Xenon lamp with a 450 nm long pass filter (160 mW cm<sup>-2</sup>) as the light source. The temperature of the system was controlled by water bath (303 ± 0.5 K) running through the outer casing of the Pyrex glass tube to avoid light induced heating. The reaction in the dark was tested under the same condition just in the absence of light. After the reaction, the suspension was separated by centrifugation, and the solution was analyzed with Shimadzu Type GC-14C equipped with a flame ionization detector, using a SGE-30QC2/AC5 capillary column and N<sub>2</sub> as carrier gas. GC-MS (Thermo Trace GC Ultra DSQ) was also employed to determine the reaction products.

## 2.5 Photoelectrochemical performance measurement

The photoelectrochemical measurements were performed using a classical three-electrode cell consisting of M/TiO<sub>2</sub>-NB nanostructures as photoanode (working electrode), Pt counter electrode and a saturated calomel reference electrode (SCE). The photocurrent response was recorded on a CHI 660C electrochemical workstation (the current density was normalized by the geometric surface area of electrode) using 0.2 M Na<sub>2</sub>SO<sub>4</sub> as the electrolyte solution. The working electrode was irradiated by a 300 W Xenon lamp with a 450 nm long pass filter.

## 3. Results and discussion

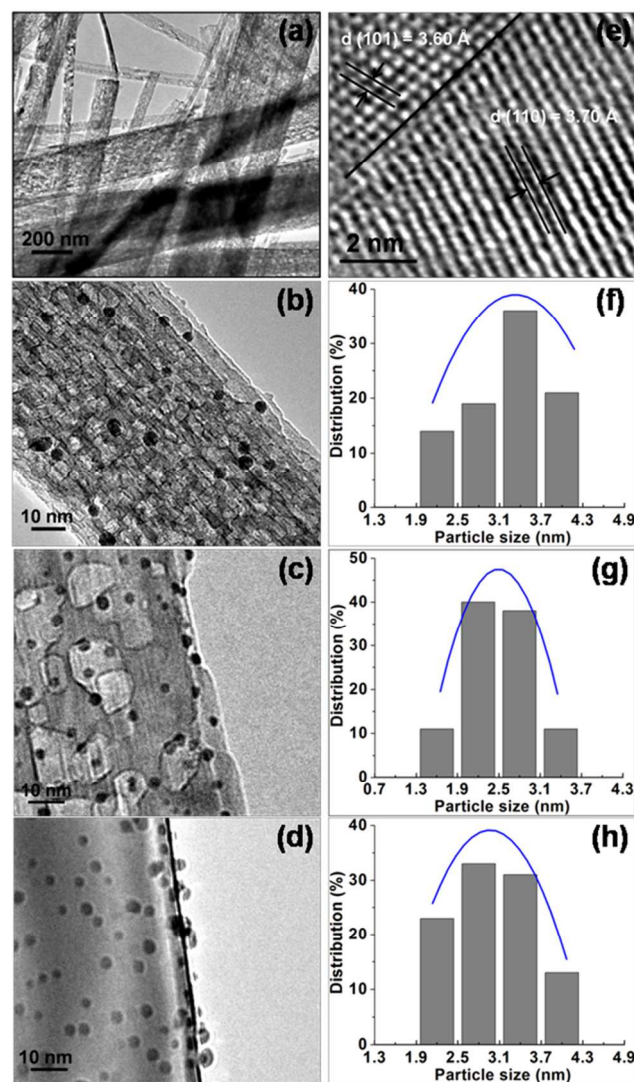


**Fig. 1** Representative TEM images of (a) TiO<sub>2</sub> nanobelts, (b) Au<sub>1</sub>/T-1, (c) Au<sub>1</sub>/T-2 and (d) Au<sub>1</sub>/T-3, and HR-TEM image of (e) T-2 nanobelt and the corresponding particle size distributions of (f) Au<sub>1</sub>/T-1, (g) Au<sub>1</sub>/T-2 and (h) Au<sub>1</sub>/T-3.

One-dimensional TiO<sub>2</sub> nanobelts with several tens of micrometers in axial direction were synthesized via the hydrothermal process (Fig. 1a). Their structure was tuned by controlling the calcination temperature of H<sub>2</sub>Ti<sub>3</sub>O<sub>7</sub> nanobelts. As shown in Fig. S1, TiO<sub>2</sub>(B) (T-1) and anatase (T-3) nanobelts were formed at 673 and 1173 K respectively, and TiO<sub>2</sub>(B)/anatase heterostructured nanobelts (T-2) with a composition of 40% TiO<sub>2</sub>(B) and 60% anatase were obtained at 873 K. The HR-TEM image (Fig. 1e) displays that two clear lattice fringes continuously spaced across the surface of T-2 nanobelts. The interplanar distances of 3.60 and 3.70 Å can be respectively indexed to (101) plane of anatase and (110) plane of TiO<sub>2</sub>(B), and the interface of the two phases is well matched.

This reveals the coherent boundary bicrystalline TiO<sub>2</sub>(B)/anatase heterostructure of T-2 nanobelts.<sup>29,32</sup> TEM observation (Fig. 1b-d) shows that large amount of small-sized Au NPs were uniformly dispersed over the surface of TiO<sub>2</sub> nanobelts in all as-synthesized Au/TiO<sub>2</sub>-NB nanostructures. The morphologies of Au/TiO<sub>2</sub>-NB nanostructure were scarcely affected by the nanobelt structure, and comparable  $d_{Au}$  (average diameter of Au NPs) values were measured for Au<sub>1</sub>/T-1 (3.3 nm), Au<sub>1</sub>/T-2 (2.8 nm) and Au<sub>3.5</sub>/T-3 (3.0 nm) (Fig. 1f-h).

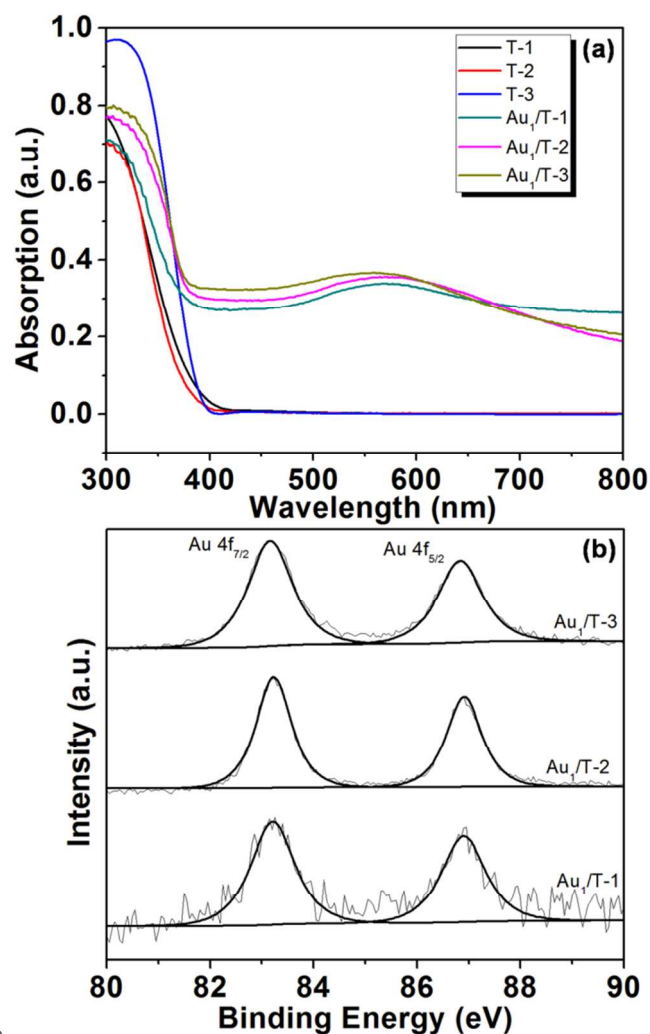


**Fig. 2** (a) Diffuse reflectance UV-vis spectra of TiO<sub>2</sub> nanobelts and Au/TiO<sub>2</sub>-NB nanostructures, and (b) XPS spectra of Au 4f in Au<sub>1</sub>/T-1, Au<sub>1</sub>/T-2 and Au<sub>1</sub>/T-3.

Fig. 2a presents the diffuse reflectance UV-vis spectra of TiO<sub>2</sub> nanobelts and Au/TiO<sub>2</sub>-NB nanostructures. In contrast to only absorption at wavelength below 450 nm for bare TiO<sub>2</sub> nanobelts, Au/TiO<sub>2</sub>-NB nanostructures showed a wide absorption peak at around 570 nm assigned to the LSPR of Au NPs.<sup>7,49</sup> XPS analysis

(Fig. 2b) reveals that the binding energies of Au 4f<sub>7/2</sub> and 4f<sub>5/2</sub> in Au/TiO<sub>2</sub>-NB nanostructures shifted to lower values (such as 83.2 and 86.9 eV in Au<sub>1</sub>/T-2) compared with the XPS data of bulk gold (84.0 and 87.7 eV). This implies that a Schottky barrier exists at Au/TiO<sub>2</sub> interface, which will lead to the electron transfer from TiO<sub>2</sub> nanobelts to Au NPs and thus gold is negatively charged.<sup>27, 50, 51</sup>

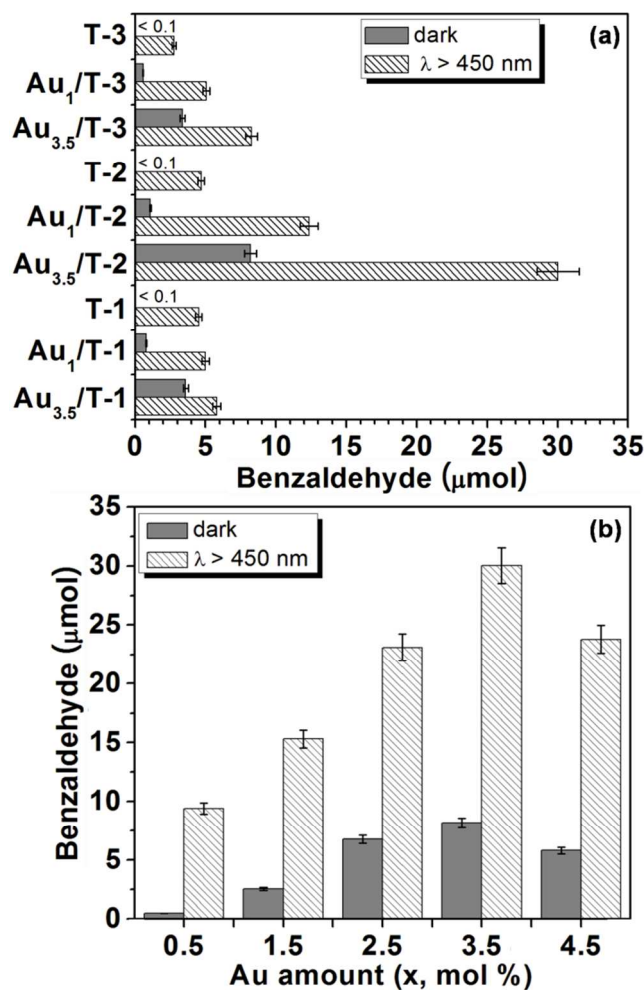


**Fig. 3** Amount of benzaldehyde formed during benzyl alcohol oxidation in the dark (grey) and under visible light irradiation (shadow) over Au/TiO<sub>2</sub>-NB photocatalysts with (a) different TiO<sub>2</sub> nanobelts and (b) different Au loadings.

The efficacy of the as-synthesized Au/TiO<sub>2</sub>-NB nanostructures for plasmonic photocatalysis was assessed by aerobic oxidation of benzyl alcohol under visible light irradiation (Xe lamp,  $\lambda > 450$  nm). Remarkably, benzyl alcohol was converted to benzaldehyde with high selectivity  $> 99\%$  over all samples, while no other products were detected. For comparison, the control experiment in the absence of photocatalysts was also performed,

and no conversion of benzyl alcohol was observed. Fig. 3a shows that all bare TiO<sub>2</sub> nanobelts exhibited no activity in the dark, while the oxidation of benzyl alcohol to benzaldehyde can be observed under visible light irradiation. This visible light driven activity can be attributed to the complex formed by the adsorption of benzyl alcohol onto TiO<sub>2</sub> surface.<sup>52-54</sup> The ligand-to-metal charge transfer of the surface complex rather than the direct excitation of TiO<sub>2</sub> should account for the visible light-promoted activity of TiO<sub>2</sub> nanobelts.<sup>55,56</sup>

It is noted that all Au/TiO<sub>2</sub>-NB nanostructures showed enhanced catalytic activity for benzyl alcohol aerobic oxidation both in the dark and under visible light irradiation. As expected, the amounts of Au loaded markedly affected the catalytic activity of Au/TiO<sub>2</sub>-NB with or without light irradiation. Take Au/T-2 catalysts for example, the amount of benzaldehyde increased monotonically with the increment of Au loading  $\leq 3.5$  mol% but decreased at higher loading in both case (Fig. 3b). The  $d_{Au}$  values for Au<sub>1</sub>/T-2, Au<sub>3.5</sub>/T-2 and Au<sub>4.5</sub>/T-2 are 2.8, 4.0 and 5.5 nm, respectively (Fig. S2, ESI<sup>†</sup>), implying that the large Au NPs with  $d_{Au} > 5$  nm are less active for reaction. Moreover, the light-promoted activity enhancement showed the same dependence on the Au loadings. The highest activity enhancement obtained over Au<sub>3.5</sub>/T-2, produced 30.1  $\mu$ mol of benzaldehyde under visible light irradiation which is 3.7 times of that obtained in the dark (8.2  $\mu$ mol).

However, the remarkable visible light-promoted activity was obtained only for Au/T-2 catalysts based on TiO<sub>2</sub>(B)/anatase heterostructured nanobelt. As is depicted in Fig. 3a, the light-promoted activity of Au/T-2 is much higher than those of Au/T-1 and Au/T-3 catalysts both with low and high Au loadings. Under visible light irradiation, Au<sub>1</sub>/T-2 produced 12.5  $\mu$ mol of benzaldehyde, while even the high-loaded Au<sub>3.5</sub>/T-1 and Au<sub>3.5</sub>/T-3 samples produced only  $< 9$   $\mu$ mol of benzaldehyde. It should be noted that the Au/TiO<sub>2</sub>-NB nanostructures based on different TiO<sub>2</sub> nanobelts are composed of comparable sized Au NPs when they are with the same Au loading (Fig. 1b-d, f-h). Obviously, the structure of TiO<sub>2</sub> nanobelts has a strong impact on the visible light-promoted activity of Au/TiO<sub>2</sub>-NB nanostructures. For Au/TiO<sub>2</sub> plasmonic photocatalysts, it has been reported that oxygen molecules adsorbed on TiO<sub>2</sub> can capture the electrons injected from Au NPs and form O-O<sup>-</sup> species which can promote the oxidation of benzyl alcohol.<sup>27</sup> We infer that the excellent visible light-promoted activity of Au/T-2 photocatalysts should

result from the efficient transfer of hot electrons from Au NPs to the heterostructured nanobelt.

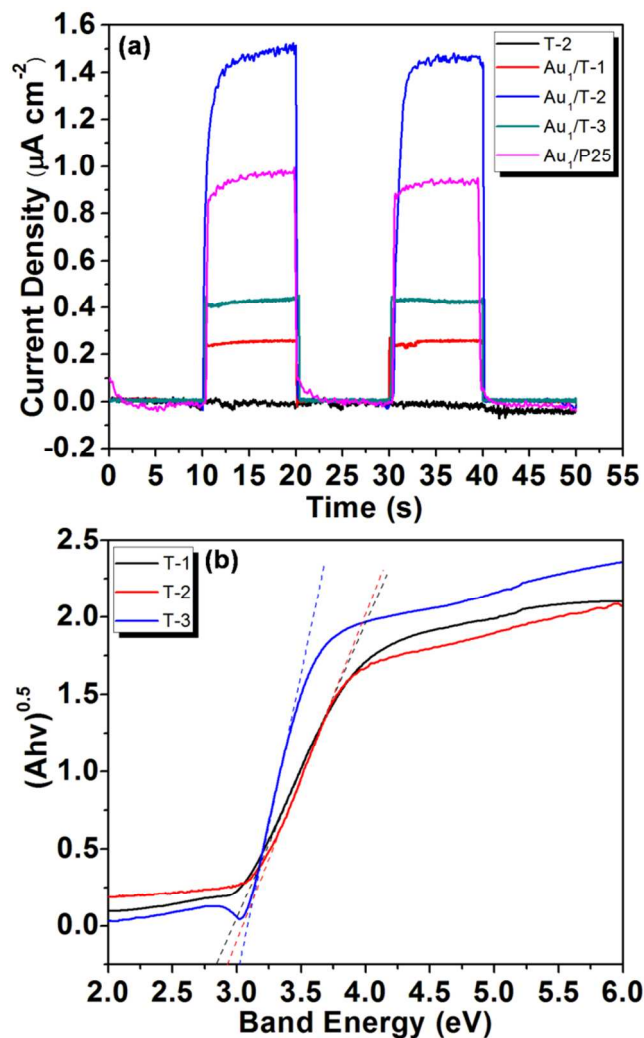


**Fig. 4** (a) The photocurrent responses of Au/TiO<sub>2</sub>-NB and Au/P25 nanostructures under visible light irradiation, and (b) plots of  $(Ah\nu)^{0.5}$  vs.  $h\nu$  of TiO<sub>2</sub> nanobelts.

In order to elucidate the role of plasmon-mediated electron transfer process in the visible light-promoted activity of Au/TiO<sub>2</sub>-NB nanostructures, a series of photoelectrochemical tests were performed. Au/TiO<sub>2</sub>-NB nanostructures and bare TiO<sub>2</sub> nanobelts were used as the working photoanodes. The I-t curves responding to light turning on and off measured at zero bias voltage are presented in Fig. 4a. As can be seen, bare TiO<sub>2</sub> nanobelts (T-2) did not produce any photocurrent signal, while all Au/TiO<sub>2</sub>-NB nanostructures exhibited significant anodic photocurrent response under visible light irradiation. For example, the measured photocurrent density is about 1.50  $\mu\text{A cm}^{-2}$  for Au<sub>1</sub>/T-2, which quickly decreased as soon as the light irradiation was stopped.

This result demonstrates that bare TiO<sub>2</sub> nanobelts indeed cannot absorb visible light with wavelength above 450 nm and produce photoinduced charge carriers. Therefore, the photocurrent responses of Au/TiO<sub>2</sub>-NB nanostructures can be attributed to the injection of hot electrons mediated via plasmonic excitation of Au NPs. It is noted that the transient photocurrent response of Au<sub>1</sub>/T-2 is much stronger than those of Au<sub>1</sub>/T-1 and Au<sub>1</sub>/T-3, indicating an efficient interfacial electron transfer between Au NPs and the heterostructured nanobelt. This photocurrent response on the respective catalysts is consistent with the catalytic activity under visible light irradiation, suggesting that the electron transfer from Au NPs to TiO<sub>2</sub> nanobelt mediated the photocatalytic activity of Au/TiO<sub>2</sub>-NB nanostructures for benzyl alcohol aerobic oxidation.

According to the UV-vis spectra of TiO<sub>2</sub> nanobelts obtained at different calcination temperatures, the band gaps of T-1, T-2 and T-3 nanobelts were calculated to be 2.83, 2.92 and 3.02 eV, respectively (Fig. 4b). This means that there should be a difference between the band structure of TiO<sub>2</sub>(B) and anatase phases, which would result in an inter-phase charge transfer when they are in contact. Up to now, the efficient charge separation and promoted photocatalytic activity have been observed for various TiO<sub>2</sub>(B)/anatase heterostructures, and several models regarding to the charge transfer in these cases have been proposed. Among them, Ke et al have demonstrated that the potentials of conduction and valence band in TiO<sub>2</sub>(B) are higher than the corresponding ones of anatase. The higher conduction band edge of TiO<sub>2</sub>(B) provides a higher Schottky barrier, which is unfavourable for the electron migration from Au NPs to TiO<sub>2</sub>, corresponding to the much lower photocurrent density of Au<sub>1</sub>/T-1 than that of Au<sub>1</sub>/T-3. The electron transfer from excited Au NPs to TiO<sub>2</sub> (< 240 fs) is much faster than the reverse process, indicating an electron accumulation in the conduction band of TiO<sub>2</sub>. This will inhibit the consecutive electron transfer from Au NPs to TiO<sub>2</sub>.

In our previous study, the heterostructured nanobelts show an anatase-TiO<sub>2</sub>(B)-anatase sandwich structure. Accordingly, for Au/T-2 samples, Au/TiO<sub>2</sub>-NB nanostructures with the heterostructured nanobelt, the HR-TEM images in Fig. S3 show that the Au NPs were mainly deposited on anatase phase. When Au/T-2 catalysts were irradiated by visible light, most of the hot electrons will be injected into the conduction band of anatase. The electron accumulation in conduction band of anatase can realign energy levels in TiO<sub>2</sub>(B)/anatase heterostructure, enabling

the electron transfer from anatase to TiO<sub>2</sub>(B). Accordingly, the TiO<sub>2</sub>(B)/anatase heterojunction enables efficient electron transport within the heterostructured nanobelt, which will in turn facilitate the injection of hot electrons from Au NPs into TiO<sub>2</sub>. This enhanced consecutive transfer of electrons between dual heterojunction contributes to the much higher photocurrent response and visible light-promoted activity of Au<sub>1</sub>/T-2 than those of Au<sub>1</sub>/T-1 and Au<sub>1</sub>/T-3 based on single-phase nanobelt.

For comparison, Au/P25 with the same Au loading was prepared and tested. The benzaldehyde formed over Au<sub>1</sub>/P25 in the dark and under visible light irradiation are 13.5 and 21.6 μmol respectively. However, the light enhanced benzaldehyde formation obtained over Au<sub>1</sub>/P25 (8.1 μmol) is lower than that over Au<sub>1</sub>/T-2 (11.3 μmol, see Fig.2a). Correspondingly, a weaker transient photocurrent response of Au<sub>1</sub>/P25 (0.95 μA cm<sup>-2</sup>) than that of Au<sub>1</sub>/T-2 (1.50 μA cm<sup>-2</sup>) was observed (Fig. 4a). This demonstrates that a more efficient electron transfer occurred in Au<sub>1</sub>/T-2, which can be ascribed to the anisotropic electron flow in the heterostructured nanobelts. Moreover, due to the one-dimensional structure of TiO<sub>2</sub> nanobelts, Au/TiO<sub>2</sub>-NB nanostructures can be easily separated from the resulting solution after reaction by sedimentation in less than 5 min, while the suspension with the Au/P25 is still turbid (Fig. S4, ESI†). This additionally suggests that TiO<sub>2</sub>(B)/anatase heterostructured TiO<sub>2</sub> nanobelt can function as an ideal support and electron transfer mediator of plasmonic Au NPs.

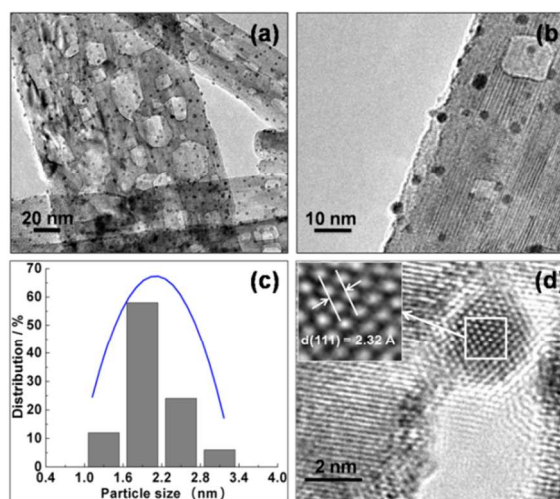


**Fig. 5** Representative (a,b) TEM and (d) HR-TEM images of Au<sub>0.75</sub>Pd<sub>0.25</sub>/T-2, and (c) its corresponding particle size distribution.

It has been shown that the photocatalytic performance of Au-

based plasmonic photocatalysts can be effectively improved by the incorporation of a second metal.<sup>43-48</sup> Herein, we synthesized a series of bimetallic Au-Pd/TiO<sub>2</sub>-NB nanostructures by the similar method used in the synthesis of Au/TiO<sub>2</sub>-NB samples. Fig. 5a,b show the representative TEM images of Au<sub>0.75</sub>Pd<sub>0.25</sub>/T-2. Just like the morphology of Au/TiO<sub>2</sub>-NB nanostructures, small-sized metal NPs were highly dispersed on the surface of TiO<sub>2</sub> nanobelts. A narrow size distribution with an average diameter of 2.1 nm was obtained. As shown in Fig. S5, the average diameters of metal NPs in Au<sub>0.5</sub>Pd<sub>0.5</sub>/T-2, Au<sub>0.25</sub>Pd<sub>0.75</sub>/T-2 and Pd<sub>1</sub>/T-2 nanostructures are 2.0, 1.9, 1.7 nm, respectively. The particle sizes of Au-Pd NPs decreased with the decrease of Au/Pd molar ratio which is in agreement with the previous report.<sup>58</sup> In addition, the HR-TEM image in Fig. 5d reveals that the metal NPs in Au<sub>0.75</sub>Pd<sub>0.25</sub>/T-2 are well-faceted and the measured lattice spacing of 2.32 Å is just between the values of Au(111) (2.35 Å in PDF No. 65-8601) and Pd(111) (2.25 Å in PDF No. 65-2867), indicative of Au-Pd alloy NPs.

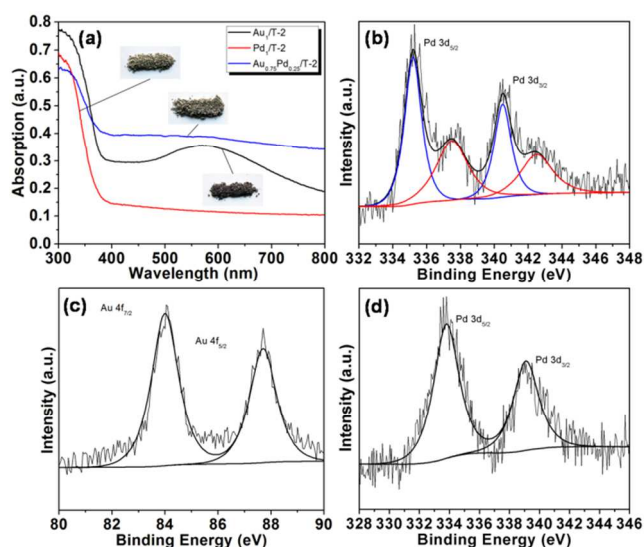


**Fig. 6** (a) Diffuse reflectance UV-vis spectra of Au<sub>1</sub>/T-2, Pd<sub>1</sub>/T-2 and Au<sub>0.75</sub>Pd<sub>0.25</sub>/T-2, and XPS spectra of (b) Pd 3d in Pd<sub>1</sub>/T-2, (c) Au 4f and (d) Pd 3d in Au<sub>0.75</sub>Pd<sub>0.25</sub>/T-2.

It is known that the characteristic absorption peak of Pd NPs is in the UV region at a wavelength of 330 nm,<sup>59-61</sup> which is overlapped by the absorption peak of TiO<sub>2</sub>. However, an increase of the baseline in the visible light region was observed for Pd<sub>1</sub>/T-2 sample compared with bare TiO<sub>2</sub> nanobelts (T-2) in Fig. 6a, which can be attributed to the light scattering or the interband electronic transitions of Pd NPs.<sup>62,63</sup> For bimetallic Au-Pd/TiO<sub>2</sub>-NB nanostructures, the Au alloyed with Pd led to the

characteristic LSPR absorption peak of Au NPs at 570 nm broadening or even disappeared, corresponding to the color change of sample from purple to gray (inserted digital pictures in Fig. 6a). The Pd 3d and Au 4f XPS spectra in Pd<sub>1</sub>/T-2 and Au<sub>0.75</sub>Pd<sub>0.25</sub>/T-2 are shown in Fig. 6b-d. It can be seen that the Pd 3d<sub>3/2</sub> peak in Pd<sub>1</sub>/T-2 could be fitted by two peaks of 340.5 and 342.5 eV which are attributed to metallic Pd and PdO species respectively.<sup>64,65</sup> The existence of PdO is due to the easy oxidation of Pd NPs upon contact with O<sub>2</sub> in air or water at room temperature. Compared to the values of Au 4f detected in Au<sub>1</sub>/T-2 (Fig. 2b), the corresponding binding energies in Au<sub>0.75</sub>Pd<sub>0.25</sub>/T-2 shifted to higher values of 84.0 and 87.7 eV, while the peak of Pd 3d<sub>3/2</sub> (339.1 eV) negatively shifted about 1.4 eV relative to the data of metallic Pd detected in Pd<sub>1</sub>/T-2. This result indicates that alloying Au with Pd gives Au a tendency to lose electrons. Given that the work function of metal Pd (5.6 eV) is larger than that of metal Au (5.3 eV), the migration of electrons from Au sites to Pd sites can occur.<sup>47,59-61</sup> The positive shift of Au 4f and negative shift of Pd 3d indicate that the redistribution of electrons occurs in Au<sub>0.75</sub>Pd<sub>0.25</sub>/T-2, charging Au positively and Pd negatively when the equilibrium reaches.

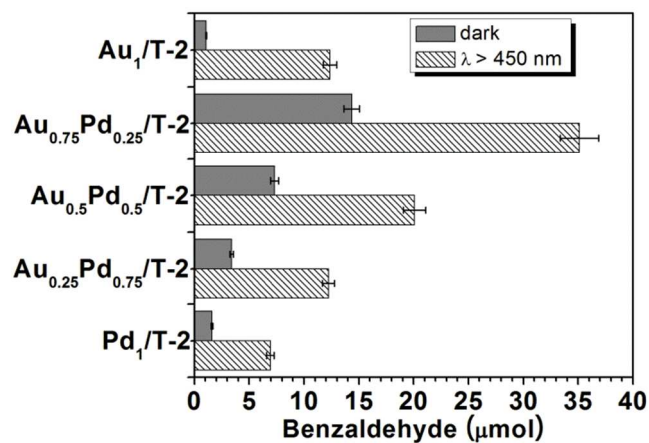


**Fig. 7** Amount of benzaldehyde formed during oxidation of benzyl alcohol over Au-Pd/T-2 photocatalysts.

The surface charge heterogeneity of Au-Pd alloy NPs will contribute to the improved catalytic performance of bimetallic nanostructures.<sup>59-61</sup> Fig. 7 indeed shows that all bimetallic Au-Pd/T-2 nanostructures exhibited enhanced catalytic activity compared to their monometallic counterparts in the dark. The Pd/T-2 sample showed slightly enhanced catalytic activity compared to bare TiO<sub>2</sub> nanobelts under visible light irradiation and no photocurrent response was observed (Fig. S6, ESI†), indicating the nonplasmonic metal nature of metal Pd. The

remarkable visible light-promoted catalytic performance was observed for all bimetallic Au-Pd/T-2 nanostructures, and the activity enhancement is strongly dependent on Au/Pd ratio. The Au<sub>0.75</sub>Pd<sub>0.25</sub>/T-2 (ICP-measured Au/Pd molar ratio is 2.4) showed the highest light-promoted activity, 35.2 μmol of benzaldehyde was produced under visible light irradiation, which is almost three times that obtained with Au<sub>1</sub>/T-2 (12.3 μmol). For Au<sub>0.5</sub>Pd<sub>0.5</sub>/T-2 and Au<sub>0.25</sub>Pd<sub>0.75</sub>/T-2 samples, even though the Au-Pd NPs sizes become smaller, the photocatalytic efficiency is still lower than that of Au<sub>0.75</sub>Pd<sub>0.25</sub>/T-2. These data suggest a plasmonic Au mediated benzyl alcohol oxidation over bimetallic nanostructures under visible light irradiation. From Fig.7, it can be seen that the light-promoted activity enhancement of Au<sub>0.75</sub>Pd<sub>0.25</sub>/T-2 is much higher than that of monometallic Au/T-2, indicative of a promoting effect of alloying Au with Pd for aerobic oxidation under visible light irradiation. This visible light-promoted synergistic effect of Au-Pd alloy NPs for benzyl alcohol oxidation can be ascribed to the charge transfer between Au and Pd, and similar findings were found for ZrO<sub>2</sub> supported Au-Pd alloy NPs photocatalysts reported by Zhu et al.<sup>59-61</sup> The redistribution of hot electrons within alloy NPs might decrease the amount of electrons injected from alloy NPs into nanobelts to some extent. It is shown that a weaker photocurrent response of 0.83 μA cm<sup>-2</sup> was measured for Au<sub>0.75</sub>Pd<sub>0.25</sub>/T-2 (Fig. S6, ESI†) compared to the value of 1.50 μA cm<sup>-2</sup> obtained for Au<sub>1</sub>/T-2, though comparable light absorptions were measured for these two nanostructures. Accordingly, less activated O-O<sup>•</sup> species is expected to be produced on TiO<sub>2</sub> nanobelts surface in Au<sub>0.75</sub>Pd<sub>0.25</sub>/T-2 as compared to the case of monometallic Au<sub>1</sub>/T-2, which would result in the decrease of benzaldehyde formation. Therefore, the remarkably improved visible-light-promoted activity obtained for Au<sub>0.75</sub>Pd<sub>0.25</sub>/T-2 suggests the synergistic effect resulted from the charge transfer in alloy NPs under visible light irradiation.

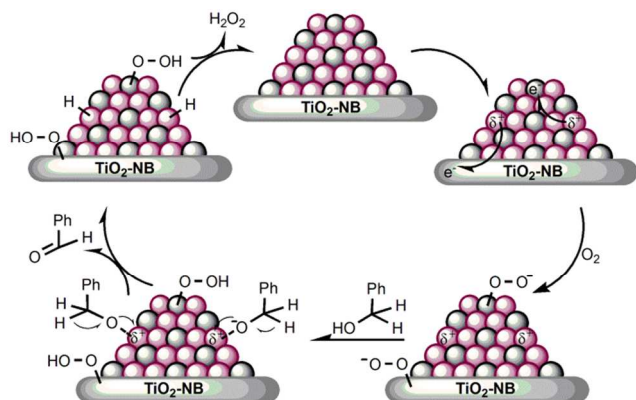


**Fig. 8** Proposed mechanism for the aerobic oxidation of benzyl alcohol over Au-Pd/T-2 nanostructures driven by visible light irradiation.

It is generally accepted that the alcohol oxidation over both Pd and Au NPs involves sequential cleavage of O-H and C-H bonds, followed by abstraction of the hydrogen atom from the intermediate of metal-hydride species.<sup>8,66,67</sup> The light-promoted catalytic activity of bimetallic Au-Pd/T-2 nanostructures can be attributed to the efficient electron transfer between alloy NPs and the heterostructured nanobelt and the redistribution of hot electrons within alloy NPs. It has been proven that the electronic structure of Pd strongly impacts its oxygen activation efficiency, and electrons transferred into Pd are tend to have substantial effects on its ability to activate oxygen molecules.<sup>68-70</sup> Therefore, the hot electrons transfer both from Au to TiO<sub>2</sub> nanobelt and to Pd sites play a key role in the activation of oxygen molecules, and facilitate the cleavage of O-H bond of the alcohol. Simultaneously, the holes left in Au sites can react with the alkoxide intermediate, accelerating the cleavage of C-H bonds.

On the basis of the results presented and discussed above, a possible mechanism for the visible light-promoted aerobic oxidation of benzyl alcohol over Au-Pd/T-2 photocatalysts is proposed in Fig. 8. It illustrates that the oxidation of benzyl alcohol proceeds through the cooperation between bimetallic Au-Pd alloy NPs and the heterostructured nanobelt. In the first step, plasmon activation of Au sites transfers hot electrons to Pd sites and the heterostructured nanobelts. The hot electrons in Pd sites and the heterostructured nanobelts can populate unoccupied orbitals of oxygen molecules yielding a transient anion O-O<sup>•</sup> species,<sup>27,71,72</sup> which can cleave the O-H bond of the alcohol to form an alkoxide intermediate. In the second step, the intermediate undergoes a rapid hydride transfer from C-H to the positive charged Au to form benzaldehyde and Au-H species.<sup>8</sup> The third step will be the elimination of Au-H species and the recovery of the active sites. The proposed mechanism gives the reasonable explanation for the light-promoted catalytic performance of bimetallic Au-Pd/T-2 nanostructures.

#### 4. Conclusions

In conclusion, deposition-precipitation method has been applied to synthesize highly dispersed small-sized Au and Au-Pd alloy NPs on TiO<sub>2</sub> nanobelts. The one-dimensional nanobelt consisting of TiO<sub>2</sub>(B)/anatase heterojunction enables efficient

transfer of hot electrons from Au NPs to TiO<sub>2</sub> nanobelts. This was confirmed by the superior visible-light-promoted activity and much higher photocurrent response of the dual heterostructured Au/(TiO<sub>2</sub>(B)/anatase) nanostructure compared to Au/TiO<sub>2</sub>(B) and Au/anatase counterparts. The bimetallic Au-Pd/TiO<sub>2</sub>-NB nanostructures showed a remarkably improved visible light driven activity compared to monometallic Au/TiO<sub>2</sub>-NB sample, which can be attributed to the plasmon-mediated charge distribution from Au sites to Pd sites within alloy NPs. We anticipate that the findings obtained here are useful in the utilization of solar energy and contribute to the design and synthesis of more efficient plasmonic photocatalysts.

## Acknowledgments

We gratefully acknowledge the financial support of the National Natural Science Foundation of China (Grant No. 51372142, 21176144, 21171106), National Science Fund for Distinguished Young Scholars (NSFDYS: 50925205), Innovation Research Group (IRG: 51321091), and the “100 Talents Program” of Chinese Academy of Sciences.

## Notes and references

<sup>a</sup> Key Laboratory of Colloid and Interface Chemistry, Ministry of Education, School of Chemistry and Chemical Engineering, Shandong University, 27 Shandan Road, Jinan 250100, China.

Email: xhxu@sdu.edu.cn

<sup>b</sup> Center for Nanochemistry, Beijing National Laboratory for Molecular Sciences, State Key Laboratory for Structural Chemistry of Unstable and Stable Species, College of Chemistry and Molecular Engineering, Peking University, Beijing 100871, China.

<sup>c</sup> State Key Laboratory of Crystal Materials, Shandong University, 27 Shandan Road, Jinan, 250100, China.

E-mail: hongliu@sdu.edu.cn

Electronic Supplementary Information (ESI) available: [details of any supplementary information available should be included here]. See DOI: 10.1039/b000000x/

1 S. Arrii, F. Morfin, A. J. Renouprez and J. L. Rousset, *J. Am. Chem. Soc.*, 2004, **126**, 1199-1205.

2 H. Y. Fan, C. Shi, X. S. Li, S. Zhang, J. L. Liu and A. M. Zhu, *Appl. Catal. B: Environ.*, 2012, **119-120**, 49-55.

3 Y. Maeda, Y. Iizuka and M. Kohyama, *J. Am. Chem. Soc.*, 2013, **135**, 906-909.

4 E. Sacaliuc, A. M. Beale, B. M. Weckhuysen and T. A. Nijhuis, *J. Catal.*, 2007, **248**, 235-248.

5 J. Huang, T. Akita, J. Faye, T. Fujitani, T. Takei and M. Haruta, *Angew. Chem. Int. Ed.*, 2009, **48**, 7862-7866.

6 C. Qi, J. Huang, S. Bao, H. Su, T. Akita and M. Haruta, *J. Catal.*, 2011, **281**, 12-20.

7 J. Huang, W. L. Dai, H. Li and K. Fan, *J. Catal.*, 2007, **252**, 69-76.

8 A. Abad, C. Almela, A. Corma and H. Garcia, *Chem. Commun.*, 2006, 3178-3180.

9 H. Liu, Y. Liu, Y. Li, Z. Tang and H. Jiang, *J. Phys. Chem. C*, 2010, **114**, 13362-13369.

10 G. M. Mullen, L. Zhang, E. J. Evans Jr, T. Yan, G. Henkelman and C. B. Mullins, *J. Am. Chem. Soc.*, 2014, **136**, 6489-6498.

11 P. K. Jain, X. Huang, I. H. El-Sayed and M. A. El-Sayed, *Acc. Chem. Res.*, 2008, **41**, 1578-1586.

12 S. Linic, P. Christopher and D. B. Ingram, *Nat. Mater.*, 2011, **10**, 911-921.

13 M. Xiao, R. Jiang, F. Wang, C. Fang, J. Wang and J. C. Yu, *J. Mater. Chem. A*, 2013, **1**, 5790-5805.

14 A. Bumajdad and M. Madkour, *Phys. Chem. Chem. Phys.*, 2014, **16**, 7146-7158.

15 R. Jiang, B. Li, C. Fang and J. Wang, *Adv. Mater.*, 2014, DOI: 10.1002/adma.201400203.

16 C. Wang and D. Astruc, *Chem. Soc. Rev.*, 2014, **43**, 7188-7216.

17 X. Wang, C. Liow, D. Qi, B. Zhu, W. R. Leow, H. Wang, C. Xue, X. Chen and S. Li, *Adv. Mater.*, 2014, **26**, 3506-3512.

18 Z. Bian, T. Tachikawa, P. Zhang, M. Fujitsuka and T. Majima, *J. Am. Chem. Soc.*, 2014, **136**, 458-465.

19 F. Su, T. Wang, R. Lv, J. Zhang, P. Zhang, J. Lu and J. Gong, *Nanoscale*, 2013, **5**, 9001-9009.

20 S. Mubeen, G. Hernandez-Sosa, D. Moses, J. Lee and M. Moskovits, *Nano Lett.*, 2011, **11**, 5548-5552.

21 J. Long, H. Chang, Q. Gu, J. Xu, L. Fan, S. Wang, Y. Zhou, W. Wei, L. Huang, X. Wang, P. Liu and W. Huang, *Energy Environ. Sci.*, 2014, **7**, 973-977.

22 A. Furube, L. Du, K. Hara, R. Katoh and M. Tachiya, *J. Am. Chem. Soc.*, 2007, **129**, 14852-14853.

23 D. C. Hurum, A. G. Agrios and K. A. Gray, *J. Phys. Chem. B*, 2003, **107**, 4545-4549.

24 T. Kawahara, Y. Konishi, H. Tada, N. Tohge, J. Nishii and S. Ito, *Angew. Chem. Int. Ed.*, 2002, **41**, 2811-2813.

25 J. Zhang, Q. Xu, Z. Feng, M. Li and C. Li, *Angew. Chem. Int. Ed.*, 2008, **47**, 1766-1769.

26 D. O. Scanlon, C. W. Dunnill, J. Buckeridge, S. A. Shevlin, A. J. Logsdail, S. M. Woodley, C. R. A. Catlow, M. J. Powell, R. G. Palgrave, I. P. Parkin, G. W. Watson, T. W. Keal, P. Sherwood, A.

- Walsh and A. A. Sokol, *Nat. Mater.*, 2013, **12**, 798-801.
- 27 D. Tsukamoto, Y. Shiraishi, Y. Sugano, S. Ichikawa, S. Tanaka  
and T. Hirai, *J. Am. Chem. Soc.*, 2012, **134**, 6309-6315.
- 28 Y. Wen, B. Liu, W. Zeng and Y. Wang, *Nanoscale*, 2013, **5**,  
5 9739-9746.
- 29 W. Zhou, L. Gai, P. Hu, J. Cui, X. Liu, D. Wang, G. Li, H.  
Jiang, D. Liu, H. Liu and J. Wang, *CrystEngComm*, 2011, **13**,  
6643-6649.
- 30 W. Li, C. Liu, Y. Zhou, Y. Bai, X. Feng, Z. Yang, L. Lu, X.  
10 Lu and K. Y. Chan, *J. Phys. Chem. C*, 2008, **112**, 20539-20545.
- 31 D. Yang, H. Liu, Z. Zheng, Y. Yuan, J. C. Zhao, E. R.  
Waclawik, X. Ke and H. Zhu, *J. Am. Chem. Soc.*, 2009, **131**,  
17885-17893.
- 32 B. Liu, A. Khare and E. S. Aydil, *ACS Appl. Mater. Interfaces*,  
15 2011, **3**, 4444-4450.
- 33 D. Yang, J. Zhao, H. Liu, Z. Zheng, M. O. Adebajo, H. Wang,  
X. Liu, H. Zhang, J. C. Zhao, J. Bell and H. Zhu, *Chem. Eur. J.*,  
2013, **19**, 5113-5119.
- 34 H. H. Lo, N. O. Gopal, S. C. Sheu and S. C. Ke, *J. Phys.*  
20 *Chem. C*, 2014, **118**, 2877-2884.
- 35 A. P. Alivisatos, *Science*, 1996, **271**, 933-937.
- 36 M. Law, J. Goldberger and P. Yang, *Annu. Rev. Mater. Res.*,  
2004, **34**, 83-122.
- 37 J. Tian, Z. Zhao, A. Kumar, R. I. Boughton and H. Liu, *Chem.*  
25 *Soc. Rev.*, 2014, **43**, 6920-6937.
- 38 Y. Guan, N. Zhao, B. Tang, Q. Jia, X. Xu, H. Liu and R. I.  
Boughton, *Chem. Commun.*, 2013, **49**, 11524-11526.
- 39 Q. Jia, D. Zhao, B. Tang, N. Zhao, H. Li, Y. Sang, N. Bao, X.  
Zhang, X. Xu and H. Liu, *J. Mater. Chem. A*, 2014, **2**, 16292-  
30 16298.
- 40 H. L. Jiang and Q. Xu, *J. Mater. Chem.*, 2011, **21**, 13705-  
13725.
- 41 D. Wang and Y. Li, *Adv. Mater.*, 2011, **23**, 1044-1060.
- 42 M. Sankar, N. Dimitratos, P. J. Miedziak, P. P. Wells, C. J.  
35 Kiely and G. J. Hutchings, *Chem. Soc. Rev.*, 2012, **41**, 8099-8139.
- 43 P. Montes-Navajas, M. Serra and H. Garcia, *Catal. Sci.*,  
*Technol.*, 2013, **3**, 2252-2258.
- 44 Y. Sugano, Y. Shiraishi, D. Tsukamoto, S. Ichikawa, S. Tanaka  
and T. Hirai, *Angew. Chem. Int. Ed.*, 2013, **52**, 5295-5299.
- 40 45 A. Zielińska-Jurek, E. Kowalska, J. W. Sobczak, W. Lisowski,  
B. Ohtani and A. Zaleska, *Appl. Catal. B: Environ.*, 2011, **101**,  
504-514.
- 46 N. Zhou, L. Polavarapu, N. Gao, Y. Pan, P. Yuan, Q. Wang and  
Q. H. Xu, *Nanoscale*, 2013, **5**, 4236-4241.
- 47 A. Tanaka, K. Fuku, T. Nishi, K. Hashimoto and H. Kominami,  
*J. Phys. Chem. C*, 2013, **117**, 16983-16989.
- 48 A. Cybula, J. B. Priebe, M. M. Pohl, J. W. Sobczak, M.  
Schneider, A. Zielińska-Jurek, A. Brückner and A. Zaleska, *Appl.*  
*Catal. B: Environ.*, 2014, **152-153**, 202-211.
- 50 49 P. Kittisakmontree, B. Pongthawornsakun, H. Yoshida, S. I.  
Fujita, M. Arai and J. Panpranot, *J. Catal.*, 2013, **297**, 155-164.
- 50 E. W. McFarland and J. Tang, *Nature*, 2003, **421**, 616-618.
- 51 J. Y. Park, H. Lee, J. R. Renzas, Y. Zhang and G. A. Somorjai,  
*Nano Lett.*, 2008, **8**, 2388-2392.
- 55 52 S. Higashimoto, N. Kitao, N. Yoshida, T. Sakura, M. Azuma,  
H. Ohue and Y. Sakata, *J. Catal.*, 2009, **266**, 279-285.
- 53 S. Higashimoto, N. Kitao, M. Azuma, H. Ohue and Y. Sakata,  
*J. Catal.*, 2010, **274**, 76-83.
- 54 C. J. Li, G. R. Xu, B. Zhang and J. R. Gong, *Appl. Catal. B:*  
60 *Environ.*, 2012, **115-116**, 201-208.
- 55 Y. Wang, K. Hang, N. A. Anderson and T. Lian, *J. Phys.*  
*Chem. B*, 2003, **107**, 9434-9440.
- 56 T. Tachikawa, S. Tojo, M. Fujitsuka and T. Majima, *Langmuir*,  
2004, **20**, 2753-2759.
- 65 57 Y. Bai, W. Li, C. Liu, Z. Yang, X. Feng, X. Lu and K. Y. Chan,  
*J. Mater. Chem.*, 2009, **19**, 7055-7061.
- 58 Y. Hong, X. Jing, J. Huang, D. Sun, T. Odoom-Wubah, F. Yang,  
M. Du and Q. Li, *ACS Sustainable Chem. Eng.*, 2014, **2**, 1752-  
1759.
- 70 59 S. Sarina, S. Bai, Y. Huang, C. Chen, J. Jia, E. Jaatinen, G. A.  
Ayoko, Z. Bao and H. Zhu, *Green Chem.*, 2014, **16**, 331-341.
- 60 S. Sarina, H. Zhu, E. Jaatinen, Q. Xiao, H. Liu, J. Jia, C. Chen  
and J. Zhao, *J. Am. Chem. Soc.*, 2013, **135**, 5793-5801.
- 61 Q. Xiao, S. Sarina, A. Bo, J. Jia, H. Liu, D. P. Arnold, Y.  
75 Huang, H. Wu and H. Zhu, *ACS Catal.*, 2014, **4**, 1725-1734.
- 62 Y. Sugano, K. Fujiwara, Y. Shiraishi, S. Ichikawa and T. Hirai,  
*Catal. Sci. Technol.*, 2013, **3**, 1718-1724.
- 63 S. Sarina, H. Y. Zhu, Q. Xiao, E. Jaatinen, J. Jia, Y. Huang, Z.  
Zheng and H. Wu, *Angew. Chem. Int. Ed.*, 2014, **53**, 2935-2940.
- 80 64 M. C. Militello, S. J. Simko, *Surf. Sci. Spectra*, 1997, **3**, 387-  
394.
- 65 M. C. Militello, S. J. Simko, *Surf. Sci. Spectra*, 1997, **3**, 395-  
401.
- 66 K. Mori, T. Hara, T. Mizugaki, K. Ebitani and K. Kaneda, *J.*  
85 *Am. Chem. Soc.*, 2004, **126**, 10657-10666.
- 67 M. Conte, H. Miyamura, S. Kobayashi and V. Chechik, *J. Am.*

---

*Chem. Soc.*, 2009, **131**, 7189-7196.

68 W. E. Kaden, T. Wu, W. A. Kunkel and S. L. Anderson,  
*Science*, 2009, **326**, 826-829.

69 W. E. Kaden, W. A. Kunkel, M. D. Kane, F. S. Roberts and S.  
5 L. Anderson, *J. Am. Chem. Soc.*, 2010, **132**, 13097-13099.

70 R. Long, K. Mao, M. Gong, S. Zhou, J. Hu, M. Zhi, Y. You, S.  
Bai, J. Jiang, Q. Zhang, X. Wu and Y. Xiong, *Angew. Chem. Int.*  
*Ed.*, 2014, **53**, 3205-3209.

71 P. Christopher, H. Xin and S. Linic, *Nat. Chem.*, 2011, **3**, 467-  
10 472.

72 P. Christopher, H. Xin, A. Marimuthu and S. Linic, *Nat. Mater.*,  
2012, **11**, 1044-1050.